Optimization Based Particle-Mesh Algorithm for High-Order and Conservative Scalar Transport

Maljaars, Jakob M.; Labeur, Robert Jan; Trask, Nathaniel A.; Sulsky, Deborah L.

DOI
10.1007/978-3-030-30705-9_23

Publication date
2020

Document Version
Accepted author manuscript

Published in
Numerical Methods for Flows - FEF 2017 Selected Contributions

Citation (APA)
Maljaars, J. M., Labeur, R. J., Trask, N. A., & Sulsky, D. L. (2020). Optimization Based Particle-Mesh Algorithm for High-Order and Conservative Scalar Transport. In H. van Brummelen, A. Corsini, S. Perotto, & G. Rozza (Eds.), *Numerical Methods for Flows - FEF 2017 Selected Contributions* (pp. 265-275). (Lecture Notes in Computational Science and Engineering; Vol. 132). SpringerOpen. https://doi.org/10.1007/978-3-030-30705-9_23

Optimization Based Particle-Mesh Algorithm for High-Order and Conservative Scalar Transport

Jakob M. Maljaars[1], **Robert Jan Labeur**[1], **Nathaniel A. Trask**[2], **and Deborah L. Sulsky**[3]

[1] Delft University of Technology
Stevinweg 1, 2600 GA Delft, The Netherlands
j.m.maljaars/r.j.labeur@tudelft.nl

[2]Sandia National Laboratories*
Albuquerque, NM 87185-1320, USA
natrask@sandia.gov

[3]The University of New Mexico
Albuquerque, NM 87131, USA
sulsky@math.unm.edu

Abstract. A particle-mesh strategy is presented for scalar transport problems which provides diffusion-free advection, conserves mass locally (i.e. cellwise) and exhibits optimal convergence on arbitrary polyhedral meshes. This is achieved by expressing the convective field naturally located on the Lagrangian particles as a mesh quantity by formulating a dedicated particle-mesh projection based via a PDE-constrained optimization problem. Optimal convergence and local conservation are demonstrated for a benchmark test, and the application of the scheme to mass conservative density tracking is illustrated for the Rayleigh-Taylor instability.

Keywords. Lagrangian-Eulerian, particle-mesh, advection equation, PDE-constraints, conservation, hybridized discontinuous Galerkin

1 Introduction

Tracing back to the particle-in-cell (PIC) method developed by Harlow and coworkers [1], hybrid particle-mesh methods attempt to combine a particle-based approach with a mesh-based approach, exploiting the distinct advantages of each framework. Hence, Lagrangian particles are conveniently used in the convective part of the problem, whereas a mesh is particularly efficient to account for the dynamic interactions between particles.

Despite many successful applications to model, e.g., dense particulate flows [2], history-dependent materials [3], and free-surface flows [4–6], some fundamental issues remain pertaining to such a hybrid

*Sandia National Laboratories is a multimission laboratory managed and operated by National Technology & Engineering Solutions of Sandia, LLC, a wholly owned subsidiary of Honeywell International Inc., for the U.S. Department of Energy's National Nuclear Security Administration under contract DE-NA0003525. This paper describes objective technical results and analysis. Any subjective views or opinions that might be expressed in the paper do not necessarily represent the views of the U.S. Department of Energy or the United States Government.

particle-mesh strategy. In particular, formulating an accurate and conservative coupling between the scattered particle data and the mesh is a non-trivial issue. Existing approaches generally either compromise conservation in favor of accuracy [3] or *vice versa* [7–9].

This contribution outlines a particle-mesh algorithm which fundamentally overcomes the aforementioned issue as it rigorously conserves the transported quantity both globally and locally (i.e. cellwise), while preserving extensions to arbitrary order accuracy. Key to the approach is the formulation of the particle-mesh projection in terms of a PDE-constrained minimization problem in such a way that, from a mesh-perspective, the transported Lagrangian particle field weakly satisfies an advection equation. The formulation for this optimization problem relies on the use of a hybridized discontinuous Galerkin (HDG) method.

For brevity, we present our method for a scalar hyperbolic conservation law on closed (i.e. no inflow or outflow through the boundaries) or periodic domains. Making combined use of particles and a mesh for this problem has the distinct advantage in that it allows handling the advection term free of any artificial diffusion. Forthcoming work will present the method in a particle-mesh operator splitting context for the advection-diffusion equation and the incompressible Navier-Stokes equations, also including in- and outflow boundaries [10].

The remainder is organized as follows. Section 2 introduces the governing equations, some definitions, and states the problem. Presenting the PDE-constrained particle mesh interaction and proving conservation constitute the main part of Section 3. In Section 4, we demonstrate the performance of the scheme in terms of accuracy and conservation, and apply the scheme for mass conservative density tracking in multiphase flows. Finally, Section 5 summarizes our findings.

2 Governing Equations and Problem Statement

2.1 Governing equations

We now define the hyperbolic conservation law on the space-time domain $\Omega \times I$ for a scalar quantity ψ_h. Under the simplifying assumption that the solenoidal advective field $\mathbf{a}\colon \Omega \times I \to \mathbb{R}^d$ has a vanishing normal component at the boundary (i.e. $\mathbf{a}\cdot\mathbf{n} = 0$ on $\partial\Omega$), this problem reads: given the initial condition $\psi^0 : \Omega \to \mathbb{R}$, find the scalar quantity $\psi : \Omega \times I \to \mathbb{R}$ such that

$$\frac{\partial \psi}{\partial t} + \nabla \cdot \mathbf{a}\psi = 0 \qquad \text{in} \quad \Omega \times I, \tag{1a}$$

$$(\mathbf{a}\cdot\mathbf{n})\psi = 0 \qquad \text{on} \quad \mathit{\Gamma}_N^0 \times I, \tag{1b}$$

$$\psi(\mathbf{x}, t^0) = \psi^0 \qquad \text{in} \quad \Omega, \tag{1c}$$

where the notation $\mathit{\Gamma}_N^0$ reflects that in the scope of this paper we only consider boundaries with vanishing normal velocity (i.e. $\mathbf{a}\cdot\mathbf{n} = 0$) for the sake of brevity. Hence, note that $\mathit{\Gamma}_N^0$ coincides with the domain boundary $\partial\Omega$. Once again, reference to upcoming work [10] is made for the more generic case, including inflow and outflow boundaries.

Problem Eq. (1) is solved using a set of scattered, Lagrangian particles, and our aim is to express fields as flux degrees of freedom on an Eulerian background mesh from this set of moving particles in an accurate and physically correct manner. To state this problem mathematically in Section 2.3, we first introduce some notation related to the Lagrangian particles and the Eulerian mesh.

2.2 Definitions

Let $\mathcal{X}_t$ define the configuration of Lagrangian particles in the domain Ω at a time instant t

$$\mathcal{X}_t := \{\mathbf{x}_p(t) \in \Omega\}_{p=1}^{N_p}, \tag{2}$$

in which $\mathbf{x}_p$ denotes the spatial coordinates of particle p, and N_p is the number of particles.
Furthermore, a Lagrangian scalar field on the particles is defined as

$$\Psi_t := \{\psi_p(t) \in \mathbb{R}\}_{p=1}^{N_p}, \tag{3}$$

where ψ_p denotes the scalar quantity associated with particle p.

Next, we define an Eulerian mesh as the triangulation $\mathcal{T} := \{K\}$ of Ω into open, non-overlapping cells K. A measure of the cell size is denoted by h_K, and the outward pointing unit normal vector on the boundary ∂K of a cell is denoted by $\mathbf{n}$. Adjacent cells K_i and K_j ($i \neq j$) share a common facet $F = \partial K_i \cap \partial K_j$. The set of all facets (including the exterior boundary facets $F = \partial K \cap \partial\Omega$) is denoted by $\mathcal{F}$.

The following scalar finite element spaces are defined on $\mathcal{T}$ and $\mathcal{F}$:

$$W_h := \left\{w_h \in L^2(\mathcal{T}),\ w_h|_K \in P_k(K)\ \forall\ K \in \mathcal{T}\right\}, \tag{4}$$

$$T_h := \left\{\tau_h \in L^2(\mathcal{T}),\ \tau_h|_K \in P_l(K)\ \forall\ K \in \mathcal{T}\right\}, \tag{5}$$

$$\bar{W}_h := \left\{\bar{w}_h \in L^2(\mathcal{F}),\ \bar{w}_h|_F \in P_k(F)\ \forall\ F \in \mathcal{F}\right\}, \tag{6}$$

in which $P(K)$ and $P(F)$ denote the spaces spanned by Lagrange polynomials on K and F, respectively, and $k \geq 1$ and $l = 0$ indicating the polynomial order. The latter is chosen to keep the discussion concise, and reference is made to [10] for the more generic case $l \geq 0$. Also, note that $\bar{W}_h$ is continuous inside cell facets and discontinuous at their borders.
Importantly, we henceforth distinguish between Lagrangian particle data and Eulerian mesh fields by using the subscripts p and h, respectively.

2.3 Problem statement

We now formulate the two core components comprising our algorithm: solving Eq. (1) in a Lagrangian, particle-based framework, and projecting the Lagrangian quantities to a locally conservative Eulerian mesh field via a particle mesh-projection.

In a Lagrangian, particle-based frame of reference, the advection problem Eq. (1) is solved straightforwardly by decomposing the problem into two ordinary differential equations for the particle scalar quantity and the particle position, given by

$$\dot{\psi}_p(t) = 0, \tag{7a}$$

$$\dot{\mathbf{x}}_p(t) = \mathbf{a}(\mathbf{x}_p(t), t), \tag{7b}$$

where $\dot{\psi}_p(t)$ and $\dot{\mathbf{x}}_p(t)$ are the total derivatives at time t of the scalar quantity and the position of particle p, respectively. From Eq. (7a) it readily follows that the scalar valued particle property remains constant over time, i.e. $\psi_p = \psi_p(0) = \psi^0(\mathbf{x}_p)$. Furthermore, any appropriate time integration method can be used to integrate Eq. (7b) in time, and will not be subject of further discussion. Finally, as a result of

our simplifying assumption that $\mathbf{a} \cdot \mathbf{n} = 0$ at the exterior boundary Γ_N^0, we do not consider the inflow and outflow of particles through exterior boundaries, and we refer to [10] for a further discussion of this topic.

Instead, we focus on the reconstruction of a locally conservative mesh field $\psi_h \in W_h$ from the scattered particle data $\psi_p \in \Psi_t$ in a subsequent particle-mesh projection step. Abstractly, this projection $\mathcal{P}_E : \Psi_t \to W_h$ can be denoted as

$$\psi_h(\mathbf{x}, t) = \mathcal{P}_E \left(\psi_p(t) \right). \tag{8}$$

Our specific aim is to formulate the projection operator $\mathcal{P}_E$ in such a way that local conservation is guaranteed, in the sense that the integral of ψ_h over each element is invariant.

3 PDE-Constrained Particle-Mesh Interaction

3.1 Formulation

In order to define the projection operator $\mathcal{P}_E$, we take as our starting point a local least squares minimization problem [9]

$$\min_{\psi_h \in W_h} \; J = \sum_p \frac{1}{2} \left(\psi_h(\mathbf{x}_p(t), t) - \psi_p \right)^2. \tag{9}$$

With W_h a discontinuous function space, this approach allows for an efficient cellwise implementation, and gives accurate results provided that the particle configuration satisfies unisolvency (Definition 2.6 in [11]) with respect to W_h. The latter requirement practically implies that the particle locations in a cell are not collinear, and the number of particles in a cell is bounded from below by the number of local basis functions. In the remainder of this work we assume that this criterion is met, so as to focus entirely on a more important issue concerning Eq. (9) in that conservation of the quantity ψ_h cannot be guaranteed *a priori*.

In order to achieve conservation, Eq. (9) is extended by imposing the additional constraint that the projection has to satisfy a hyperbolic conservation law in a weak sense. To cast this into an optimization problem, the functional in Eq. (9) is augmented with terms multiplying Eq. (1a) with a Lagrange multiplier $\lambda_h \in T_h$. After integration by parts and exploiting that gradients of the Lagrange multiplier vanish on K for $l = 0$, the minimization problem may be stated: given a particle field $\psi_p \in \Psi_t$, and a solenoidal velocity field $\mathbf{a}$, find the stationary points of the Lagrangian functional

$$\begin{aligned} \mathcal{L}(\psi_h, \bar{\psi}_h, \lambda_h) = \sum_p \frac{1}{2} \left(\psi_h(\mathbf{x}_p(t), t) - \psi_p(t) \right)^2 + \sum_K \oint_{\partial K} \frac{1}{2} \beta \left(\bar{\psi}_h - \psi_h \right)^2 \mathrm{d}\Gamma \\ + \int_\Omega \frac{\partial \psi_h}{\partial t} \lambda_h \mathrm{d}\Omega + \sum_K \oint_{\partial K \setminus \Gamma_N^0} \mathbf{a} \cdot \mathbf{n} \bar{\psi}_h \lambda_h \mathrm{d}\Gamma + \oint_{\Gamma_N^0} \mathbf{a} \cdot \mathbf{n} \psi_h \lambda_h \mathrm{d}\Gamma, \end{aligned} \tag{10}$$

The first two terms at the right-hand side in this equation are recognized as a regularized least squares projection, and the last three terms constitute a weak form of the advection problem Eq. (1), with the Lagrange multiplier $\lambda_h \in T_h$ as the weight function. Furthermore, the unknown facet-based field $\bar{\psi}_h \in \bar{W}_h$, resulting from integration by parts, determines the interface flux, and is crucial in providing the required optimality control. The additional term containing $\beta > 0$ penalizes the jumps between ψ_h and

$\bar{\psi}_h$ on cell interfaces, thereby avoiding the problem of becoming singular in cases with vanishing normal velocity $\mathbf{a} \cdot \mathbf{n}$.

Equating the variations of Eq. (10) with respect to the three unknowns $(\psi_h, \lambda_h, \bar{\psi}_h) \in (W_h, T_h, \bar{W}_h)$ to zero yields the semi-discrete optimality system. An in-depth derivation can be found in [10]. Here we suffice to present the resulting fully-discrete system, thus assuming that the particle field $\psi_p \in \Psi_t$, the particle positions $\mathbf{x}_p^{n+1} \in \mathcal{X}_t$ after the Lagrangian advection, and the mesh field at the previous time level $\psi_h^n \in W_h$ are known.
Variation with respect to the scalar field $\psi_h^{n+1} \in W_h$ yields the co-state equation

$$\sum_p \left(\psi_h^{n+1}(\mathbf{x}_p^{n+1}) - \psi_p\right) w_h(\mathbf{x}_p^{n+1}) - \sum_K \oint_{\partial K} \beta \left(\bar{\psi}_h^{n+1} - \psi_h^{n+1}\right) w_h \mathrm{d}\Gamma + \int_\Omega \frac{w_h}{\Delta t} \lambda_h^{n+1} \mathrm{d}\Omega + \oint_{\Gamma_N^0} \mathbf{a} \cdot \mathbf{n} \lambda_h^{n+1} w_h \mathrm{d}\Gamma = 0 \quad \forall w_h \in W_h. \tag{11a}$$

Variation with respect to the Lagrange multiplier $\lambda_h^{n+1} \in T_h$ yields the discrete state equation

$$\int_\Omega \frac{\psi_h^{n+1} - \psi_h^n}{\Delta t} \tau_h \mathrm{d}\Omega + \sum_K \oint_{\partial K \setminus \Gamma_N^0} \mathbf{a} \cdot \mathbf{n} \bar{\psi}_h^{n+1} \tau_h \mathrm{d}\Gamma + \oint_{\Gamma_N^0} \mathbf{a} \cdot \mathbf{n} \psi_h^{n+1} \tau_h \mathrm{d}\Gamma = 0 \quad \forall \tau_h \in T_h. \tag{11b}$$

And variation with respect to the facet variable $\bar{\psi}_h^{n+1} \in W_h$ results in the optimality condition

$$\sum_K \oint_{\partial K} \mathbf{a} \cdot \mathbf{n} \lambda_h^{n+1} \bar{w}_h \mathrm{d}\Gamma + \sum_K \oint_{\partial K} \beta \left(\bar{\psi}_h^{n+1} - \psi_h^{n+1}\right) \bar{w}_h \mathrm{d}\Gamma = 0 \qquad \forall \bar{w}_h \in \bar{W}_h. \tag{11c}$$

Solving Eq. (11) for $(\psi_h^{n+1}, \lambda_h^{n+1}, \bar{\psi}_h^{n+1}) \in (W_h, T_h, \bar{W}_h)$ yields the reconstructed field $\psi_h^{n+1} \in W_h$.

3.2 Conservation

Next, we will show that from the perspective of the Eulerian field the particle-mesh projection via Eq. (11) indeed conserves mass, both in a global and a local sense. To this end, consider the discrete state equations (Eq. (11b)) and set $\tau_h = 1$. Exploiting the single-valuedness of the facet flux variable $\bar{\psi}$ at the facets $F \in \mathcal{F}$, we readily obtain

$$\int_\Omega \frac{\psi_h^{n+1} - \psi_h^n}{\Delta t} \mathrm{d}\Omega = -\sum_K \oint_{\partial K \setminus \Gamma_N^0} \mathbf{a} \cdot \mathbf{n}\, \bar{\psi}_h^{n+1} \mathrm{d}\Gamma - \oint_{\Gamma_N^0} \mathbf{a} \cdot \mathbf{n}\, \psi_h^{n+1} \mathrm{d}\Gamma = 0, \tag{12}$$

where we made use of the fact that the flux term vanishes at opposing sides of interior facets, and the flux at facets on the exterior boundary vanishes due to our earlier simplification that $\mathbf{a} \cdot \mathbf{n} = 0$ on Γ_N^0.
Local mass conservation follows when setting $\tau_h = 1$ on an interior cell K and $\tau_h = 0$ on $\Omega \setminus K$, resulting in

$$\int_K \frac{\psi_h^{n+1} - \psi_h^n}{\Delta t} \mathrm{d}\Omega = -\oint_{\partial K} \mathbf{a} \cdot \mathbf{n} \bar{\psi}_h^{n+1} \mathrm{d}\Gamma. \tag{13}$$

Thus, the storage over an element balances the net ingoing advective flux through the cell boundary ∂K which proves local conservation in terms of the numerical flux on $\mathcal{F}$.

3.3 Numerical implementation

The optimality system Eq. (11) leads to a seemingly large global system. However, this system is amenable to an efficient implementation via static condensation by eliminating the unknowns local to a cell, i.e. $(\psi_h, \lambda_h) \in (W_h, T_h)$, in favor of the global control variable $\bar{\psi}_h^{n+1} \in \bar{W}_h$, leading to a much smaller global system which is to be solved for $\bar{\psi}_h^{n+1}$ only. The local unknowns ψ_h^{n+1} and λ_h^{n+1} can be found in a subsequent backsubstitution step [9, 12].

We emphasize that our PDE-constrained particle-mesh projection hinges on the single-valued facet flux variable $\bar{\psi}_h$, acting as the control variable to our optimization procedure. This imperative ingredient is naturally provided by employing a HDG-framework (see, e.g., [12–14]).

4 Numerical Examples

In Section 4.1, the convergence and conservation of the scheme is studied for a benchmark test for which an analytical solution is available. Section 4.2 illustrates how the scheme can be applied as a tool for mass conservative density tracking in multiphase flows.

4.1 Convergence study: translation of periodic pulse

Following LeVeque [15], the translation of a sinusoidal profile $\psi(\mathbf{x}, 0) = \sin 2\pi x \sin 2\pi y$ on the bi-periodic unit square is considered. The velocity field $\mathbf{a} = [1, 1]^\top$ is used, so that at $t = 1$ the initial data should be recovered. The β-parameter is set to 1e-6, and a simple Euler scheme suffices for exact particle advection. Using different polynomial orders $k = 1, 2, 3$, the accuracy of the method is assessed at $t = 1$ by refining the mesh and the time step. We assign approximately a safe number of 28 particles per cell initially in order to comply with the unisolvency criterion. Furthermore, the time step corresponds to a CFL-number of approximately 1. The errors as well as the convergence rates are tabulated in Table 1. Optimal convergence rates of order $k + 1$ are observed, thus revealing the accuracy of our approach.

Table 1: Translating pulse: overview of model runs with the associated L^2-error $\|\psi - \psi_h\|$, the convergence rate and the local mass conservation error $\epsilon_{\Delta\phi_K}$ at time $t = 1$.

		$(k,l) = (1,0)$			$(k,l) = (2,0)$			$(k,l) = (3,0)$		
Cells	Δt	Error	Rate	$\epsilon_{\Delta\phi_K}$	Error	Rate	$\epsilon_{\Delta\phi_K}$	Error	Rate	$\epsilon_{\Delta\phi_K}$
128	0.1	6.0e-2	-	1.3e-15	4.3e-3	-	4.5e-15	3.3e-4	-	1.3e-15
512	0.05	1.6e-2	1.9	7.7e-16	5.5e-4	3.0	3.1e-16	2.1e-5	4.0	7.1e-16
2048	0.025	3.9e-3	2.0	4.3e-16	6.9e-5	3.0	2.5e-16	1.3e-6	4.0	4.4e-16
8192	0.0125	9.8e-4	2.0	2.7e-16	8.6e-6	3.0	2.3e-16	8.2e-8	4.0	3.5e-16

Table 1 also shows the local mass conservation error at $t = 1$, with this error for a time level $n + 1$

being defined as

$$\epsilon_{\Delta\phi_K} = \left(\sum_K \left(\int_K \frac{\psi_h^{n+1} - \psi_h^n}{\Delta t} \mathrm{d}\Omega + \oint_{\partial K} \mathbf{a} \cdot \mathbf{n} \bar{\psi}_h^{n+1} \mathrm{d}\Gamma \right)^2 \right)^{1/2} . \tag{14}$$

As expected, mass is conserved locally in terms of the facet flux. Global mass conservation is readily verified by noting that the facet flux term cancels at opposing sides of the facets.

4.2 Application: mass conservative Rayleigh-Taylor instability

We next illustrate how the above presented scheme can be used for a mass conservative multiphase scheme in which particles are used for the tracking of sharp interfaces. As an example, we take the Rayleigh-Taylor instability test from [16] with an Atwood number of 0.5 and a Reynolds number of 256. In addition to a PDE-constrained particle-mesh strategy for tracking the density fields, we also track specific momentum at the particle level and enforce incompressibility and viscous forces via a Stokes step at the mesh. Details of such a particle-mesh operator splitting approach for the Navier-Stokes equations can be found in [10]. A regular and symmetric mesh with $60 \times 240 \times 4$ cells is used. Initially, approximately 20 particles per cell are assigned, and we note that advecting the particles through a pointwise divergence free velocity field obviates the need for a particle reseeding strategy [9, 10]. Furthermore, we use polynomial orders $(k, l) = (1, 0)$ and use a timestep $\Delta t =$ 1e-3. Particles are advected using an explicit, three-stage Runge-Kutta scheme [17]. The evolution of the initial perturbation is visually assessed in Fig. 1. The sharp interface between the two phases is maintained and the interface shape is qualitatively in good agreement with [16]. Most importantly, computations confirm that the total mass remains constant to machine precision.

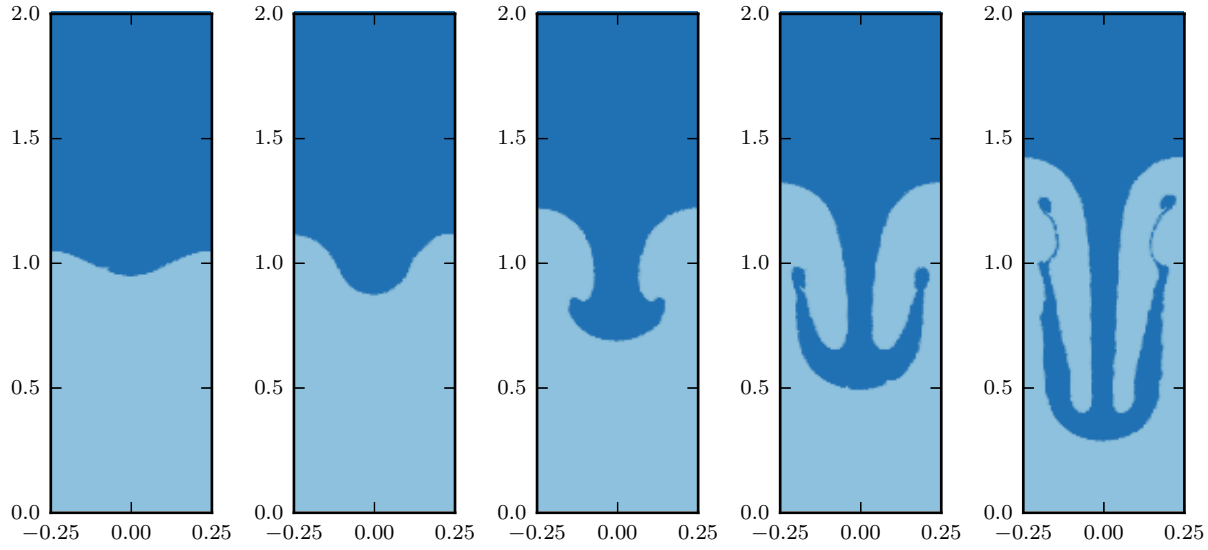

(a) t = 0 (b) t=0.25 (c) t=0.5 (d) t=0.75 (e) t= 1.0

Figure 1: Rayleigh-Taylor: time evolution of density field at particle level for Re=256.

5 Conclusions

We outlined a particle-mesh projection which enables the reconstruction of high-order accurate and diffusion-free mesh fields from a set of scattered Lagrangian particles. By casting the problem as a PDE-constrained optimization problem rigorous discrete conservation principles can be derived. Importantly, in the presented optimization strategy the advective flux was expressed in terms of a flux variable at the facet which provides the required optimality control. Such a facet function is typical to an HDG approach, and comes with the additional benefit that the resulting scheme can be implemented efficiently via static condensation. The scheme was assessed in terms of accuracy and conservation, and we highlighted a potential application to multiphase flows.

References

[1] Evans, M., Harlow, F., and Bromberg, E., The particle-in-cell method for hydrodynamic calculations, Tech. rep., Los Alamos Scientific Laboratory (1957).

[2] Snider, D., An Incompressible Three-Dimensional Multiphase Particle-in-Cell Model for Dense Particle Flows, J. Comput. Phys. 170 (2) (2001) 523–549. doi:10.1006/jcph.2001.6747.

[3] Sulsky, D., Chen, Z., and Schreyer, H., A particle method for history-dependent materials, Comput. Methods Appl. Mech. Eng. 118 (1-2) (1994) 179–196. doi:10.1016/0045-7825(94)90112-0.

[4] Zhu, Y. and Bridson, R., Animating sand as a fluid, ACM Trans. Graph. 24 (3) (2005) 965. doi:10.1145/1073204.1073298.

[5] Kelly, D. M., Chen, Q., and Zang, J., PICIN: a particle-in-cell solver for incompressible free surface flows with two-way fluid-solid coupling, SIAM J. Sci. Comput. 37 (3) (2015) 403 – 424. doi:10.1137/140976911.

[6] Maljaars, J., Labeur, R. J., Möller, M., and Uijttewaal, W., A Numerical Wave Tank Using a Hybrid Particle-mesh Approach, Proc. Eng. 175 (2017) 21–28. doi:10.1016/j.proeng.2017.01.007.

[7] Edwards, E. and Bridson, R., A high-order accurate particle-in-cell method, Int. J. Numer. Methods Eng. 90 (9) (2012) 1073–1088. doi:10.1002/nme.3356.

[8] Sulsky, D. and Gong, M., Improving the Material-Point Method, in: Innovative Numerical Approaches for Multi-Field and Multi-Scale Problems, Springer International Publishing, 2016, pp. 217–240. doi:10.1007/978-3-319-39022-2_10.

[9] Maljaars, J. M., Labeur, R. J., and Möller, M., A hybridized discontinuous Galerkin framework for high–order particle–mesh operator splitting of the incompressible Navier–Stokes equations, J. Comput. Phys. 358 (2018) 150–172. doi:10.1016/j.jcp.2017.12.036.

[10] Maljaars, J. M., Labeur, R. J., Trask, N. A., and Sulsky, D., Constrained particle-mesh projections in a hybridized discontinuous Galerkin framework with applications to advection-dominated flows (2018). arXiv:1806.09916.

[11] Wendland, H., Scattered data approximation, Vol. 17, Cambridge University Press, 2004.

[12] Rhebergen, S. and Wells, G. N., Analysis of a Hybridized/Interface Stabilized Finite Element Method for the Stokes Equations, SIAM J. Numer. Anal. 55 (4) (2017) 1982–2003. doi:10.1137/16M1083839.

[13] Wells, G. N., Analysis of an Interface Stabilized Finite Element Method: The Advection-Diffusion-Reaction Equation, SIAM J. Numer. Anal. 49 (1) (2011) 87–109. doi:10.1137/090775464.

[14] Labeur, R. J. and Wells, G. N., Energy stable and momentum conserving hybrid finite element method for the incompressible Navier–Stokes equations, SIAM J. Sci. Comput. 34 (2) (2012) 889–913. doi:10.1137/100818583.

[15] LeVeque, R. J., High-Resolution Conservative Algorithms for Advection in Incompressible Flow, SIAM J. Numer. Anal. 33 (2) (1996) 627–665. doi:10.1137/0733033.

[16] He, X., Chen, S., and Zhang, R., A Lattice Boltzmann Scheme for Incompressible Multiphase Flow and Its Application in Simulation of Rayleigh–Taylor Instability, J. Comput. Phys. 152 (2) (1999) 642 – 663. doi:10.1006/jcph.1999.6257.

[17] Ralston, A., Runge-Kutta Methods with minimum error bounds, Math. Comput. 16 (80) (1962) 431–437. doi:10.2307/2003133.